

1 **Validating SMAP SSS with in situ measurements**

2 Wenqing Tang¹, Alexander Fore¹, Simon Yueh¹, Tong Lee¹, Akiko Hayashi¹,
3 Alejandra Sanchez-Franks², Brian King², Dariusz Baranowski¹, and Justino Martinez³

4

5 ¹Jet Propulsion Laboratory, California Institute of Technology, Pasadena, CA, USA

6 ²National Oceanography Centre, Southampton, UK

7 ³Institut de Ciències del Mar, CSIC, Barcelona, Spain

8

9

10

11 **Abstract**

12

13 Sea surface salinity (SSS) retrieved from SMAP radiometer measurements is validated
14 with in situ salinity measurements collected from Argo floats, tropical moored buoys and
15 ship-based thermosalinograph (TSG) data. SMAP SSS achieved accuracy of 0.2 PSU on a
16 monthly basis in comparison with Argo gridded data in the tropics and mid-
17 latitudes. In tropical oceans, time series comparison of salinity measured at 1 m by
18 moored buoys indicates that SMAP can track large salinity changes occurred within a
19 month. Synergetic analysis of SMAP, SMOS and Argo data allows us to identify and
20 exclude erroneous jumps or drift in some real-time buoy data from assessment of
21 satellite retrieval. The resulting SMAP-buoy matchup analysis leads to an average
22 standard deviation of 0.22 PSU and correlation coefficient of 0.73 on weekly scale; the
23 average standard deviation reduced to 0.17 PSU and the correlation improved to 0.8 on
24 monthly scale. SMAP L3 daily maps reveals salty water intrusion from the Arabian Sea
25 into the Bay of Bengal during the Indian summer monsoon, consistent with the daily

26 measurements collected from floats deployed during the Bay of Bengal Boundary Layer
27 Experiment (BoBBLE) project field campaign. In the Mediterranean Sea, the spatial
28 pattern of SSS from SMAP is confirmed by the ship-based TSG data.

29

30 Key Words: SMAP, Sea Surface Salinity, Argo float, moored buoy

31

32

33

34

35

36 **1. Introduction**

37

38 The spacebased observation of sea surface salinity (SSS) is crucial for the global water
39 cycle studies. The L-band microwave technology has been used to measure the sea
40 surface salinity (SSS) on two satellite missions: the NASA's Aquarius [Le Vine et al.,
41 2007; Lagerloef et al., 2008] and the ESA's Soil Moisture and Ocean Salinity (SMOS)
42 [Kerr et al., 2010; Font et al., 2010]. The third satellite carrying L-band instruments, the
43 NASA Soil Moisture Active Passive (SMAP) observatory, is designed to measure the soil
44 moisture over land [Entekhabi et al., 2010]. Although the primary goal of SMAP is over
45 land, its measurements can also be used to retrieve SSS.

46 The measurement principle is based on the L-band microwave sensitivity to water
47 salinity, which influences the water dielectric constant and consequently the sea surface
48 emissivity measured as surface brightness temperature (T_B) by radiometer. To accurately
49 retrieve SSS from measured T_B , other factors which also contribute to the surface
50 emissivity need to be accurately accounted for through the so-called "roughness
51 correction". This is achieved through a geophysical model function (GMF) that links the
52 excess surface emissivity to ancillary geophysical parameters, including surface wind
53 speed, direction, significant wave height (SWH), and sea surface temperature (SST). The
54 L-band radar on board of Aquarius played a significant role in the roughness correction
55 as implemented in the combined active and passive (CAP) retrieval algorithm [Yueh et
56 al., 2013; Yueh et al., 2014; Tang et al., 2013; Tang et al. 2015]. The challenge for the
57 operational SMAP SSS retrieval is that it has to rely on radiometer measurements only,
58 after the unfortunate failure of SMAP radar in July 2015, a few months after launch.

59 The algorithm to retrieve SSS from SMAP radiometer data has been developed at
60 the Jet Propulsion Laboratory (JPL) [Fore et al., 2016]. Analyzing available SMAP and
61 matchup ancillary data, it is found that SMAP T_B well corroborates the Aquarius GMFs
62 for wind speed up to at least 40 m s^{-1} [Yueh et al., 2016]. Therefore, the roughness
63 correction which removes excess surface emissivity from SMAP-measured T_B is
64 currently based on the Aquarius radiometer GMF. The JPL SMAP T_B -only processing
65 uses a maximum-likelihood method to minimize the objective function, which is the
66 square sum of the differences between measured and modeled T_B for each “flavor” (i.e.
67 H-fore, H-aft, V-fore, and V-aft) [Eq. (1) in Fore et al. 2016]. An additional term is
68 included in the objective function to constrain the wind speed within a certain range of
69 ancillary wind speed from the National Centers for Environmental Prediction (NCEP).
70 The salinity is unconstrained except to restrict the valid retrieval between 0 and 40 PSU
71 (practical salinity unit). The SMAP SSS product is available for publicly access
72 (<ftp://sealion.jpl.nasa.gov/pub/outgoing/smap/v3.0> or ourcoean.jpl.nasa.gov).

73 In this paper, we validate JPL SMAP SSS product by comparison with in situ
74 measurements, which are described in Section 2. Validation results are presented in
75 Section 3 and conclusion given in Section 4.

76 77 **2. Data**

78 The SMAP SSS product analyzed in this study is the version v3.0 Level 3 (L3)
79 data produced by the radiometer T_B -only processing [Fore et al., 2016]. The SMAP Level
80 2 (L2) SSS and wind speed are retrieved at each of the salinity-wind-cell (SWC) defined
81 along the satellite swath with 1624×76 cells along/cross track per satellite revolution. The
82 L2 data covers global ocean in 8 days with a spatial resolution of $\sim 40 \text{ km}$. There are two
83

84 L3 products, monthly and 8-days, both on $0.25^\circ \times 0.25^\circ$ grid. The 8-days product is
85 created daily by averaging 8 days of L2 data centered at noon UTC (Coordinated
86 Universal Time) of the day with a search radius of 45 km and Gaussian weighting half-
87 power distance of 30 km.

88 The Argo array has approximately 3700 floats in the global ocean measuring
89 salinity and temperature profiles [Roemmich and the Argo Team, 2009], with data made
90 freely available by the International Argo Program (see Acknowledgement for data links).
91 We use two objectively interpolated (OI) gridded monthly Argo dataset produced,
92 respectively from the Scripps Institution of Oceanography (SIO)
93 (http://www.argo.ucsd.edu/Gridded_fields.html) and from the Asia-Pacific Data-
94 Research Center (APDRC) of the International Pacific Research Center (IPRC) at the
95 University of Hawaii (<http://apdrc.soest.hawaii.edu>). The SMAP L3 monthly data is
96 compared with Argo OI salinity at the shallowest depth (2.5 m) produced using individual
97 float measurements within 5 m from the surface.

98 The moored buoy arrays provide salinity measurements close to the surface (~
99 1m) at high temporal resolution in tropical oceans, which include the Tropical
100 Atmosphere Ocean (TAO)/TRITON array in the Pacific [McPhaden, 1995; McPhaden et
101 al., 1998], the Pilot Research Moored Array in the Tropical Atlantic (PIRATA) [Servain
102 et al., 1998; Bourles et al., 2008], and the Research Moored Array for Africa-Asian-
103 Australian Monsoon Analysis and Prediction (RAMA) in the Indian Ocean [McPhaden
104 et al., 2009]. The buoy salinity sensors record temperature and conductivity data at 10-
105 minute intervals, which are used to compute hourly averaged salinity with an accuracy of
106 0.02 PSU [Freitag et al., 1999]. The depths at which salinity measurements are available

107 vary with buoy locations. In this study, we only use the salinity measurements obtained
108 within 1 m from the surface to assess whether SMAP L3 SSS accurately depict the
109 changes occurred at weekly time scales to complement the analysis based on monthly
110 Argo-gridded products.

111 We also explore other in situ salinity measurements in the SMAP period particularly
112 in coastal oceans and marginal seas to complement Argo floats and moored buoys. One
113 such source is the salinity data collected by ships assembled by the Global Ocean Surface
114 Underway Data (GOSUD) Project (<http://gosud.org>) under the Intergovernmental
115 Oceanographic Commission (IOC). Specifically valuable to this study is the large amount
116 of salinity data made available by GOSUD in the Mediterranean Sea where SMAP
117 appears to be able to provide SSS retrievals. We also examined the in situ measurements
118 in the Mediterranean Sea available from the Copernicus (HCMR), an earth observing
119 data center under the European Commission (<http://copernicus.eu>).

120 Another special data set recently made available to us is from the Bay of Bengal
121 Boundary Layer Experiment (BoBBLE) project field campaign, which took place June-
122 July 2016 [Matthews et al., 2015]. During this field campaign, 7 Argo floats were
123 deployed in the southern Bay of Bengal along 8°N, between 85.3°E and 89°E. Of
124 particular interest to this study is the daily near surface salinity measurements from the
125 BoBBLE floats equipped with SeaBird (SBE) 41-CP Conductivity, Temperature and
126 Depth (CTD) sensor and Surface Temperature Salinity (STS) sensor, which is a
127 secondary free-flushed conductivity sensor used in conjunction with the CTD for
128 extending the temperature and salinity measurements through the sea surface [Larson et
129 al., 2008]. The STS returns very high-resolution salinity profile with multiple

130 measurements at 0.1 dbar pressure increment in the top one meter from the surface. For
131 this study, we average measurements obtained at pressure less than 0.5 dbar.

132 SMOS SSS, which was validated [Boutin et al, 2012; Boutin et al., 2016], is used as
133 an independent dataset for comparison in this study. We obtained SMOS salinity data
134 from the Ocean Salinity Expertise Center (CECOS) of the CNES-IFREMER, France.
135 SMOS L3 gridded data is available in 10 Days/monthly composites. SMOS data used in
136 this study is the “research” product before May 2015, and “operational” product
137 afterwards.

138
139 **3. Results**
140

141 Figure 1 presents the monthly SSS maps of May 2015 for SMAP, Aquarius,
142 SMOS and SIO Argo. The large-scale features of the salinity fields agree very well

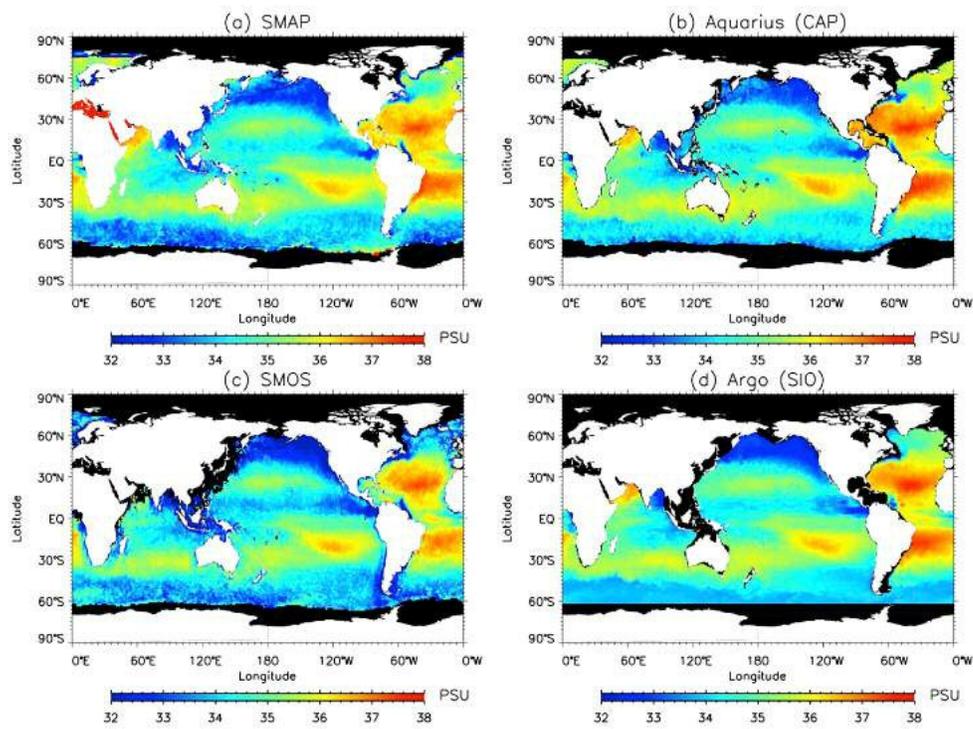


Figure 1. Global maps of sea surface salinity from (a) SMAP, (b) Aquarius (CAP), (c) SMOS and (d) Argo from SIO for the month of May 2015.

143 between satellites and Argo. We note some new details that SMAP SSS can provide close
 144 to land due to its higher spatial resolution than Aquarius and Argo and better built-in
 145 radio frequency interference (RFI) detection than Aquarius and SMOS [Mohammed et al.,
 146 2016]. Many places where no valid data from Aquarius or SMOS gridded products or
 147 Argo OI products, SMAP appears to depict reasonable SSS structure, for example, the
 148 extremely salty Mediterranean, Red Sea and the northern tip of the Arabian Sea, the fresh

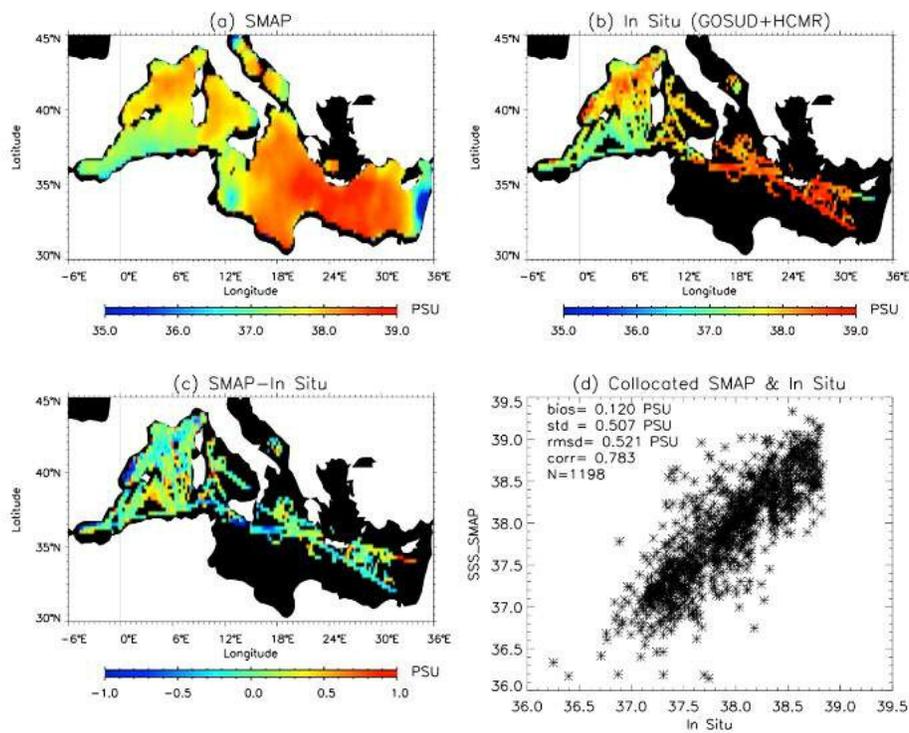


Figure 2. Sea surface salinity in the Mediterranean Sea from (a) SMAP and (b) in situ measurements bin-averaged on 0.25° grid for the period from April 1, 2015 to September 30, 2016. (c) The difference of SMAP minus in situ. (d) Scatter plot of SMAP vs. in situ over collocated grid points.

149 water on the west side of Pacific along the Kuroshio current, the northward diffusion of
 150 the Amazon river runoff plume, and the major river outflows into the coastal regions of
 151 Gulf of Mexico [Fournier et al., 2016].

152 The potential of SMAP for SSS retrieval in the Mediterranean Sea is indicated in
153 Fig. 2. The known regions with persistent RFI are on the eastern part of the
154 Mediterranean adjacent to Syria, Lebanon and Israel and the coast of Libya near Tripoli
155 (See Fig. 13 in Mohammed et al., 2016), which cause lower than expected SMAP
156 salinities (color coded as light or deep blue in Fig. 2a). Searching through the GOSUD
157 database, we found more than 300,000 sea surface salinity measurements from TSG
158 along ship trajectories in the Mediterranean Sea for the period from April 2015 to Sept.
159 2016, most of them concentrated in the western Mediterranean with two tracks across the
160 basin. We also found some glider and moored buoy data from the Copernicus marine
161 database, which extended the in situ data coverage in the eastern Mediterranean Sea.
162 Combining data from GOSUD and Copernicus, we created the daily bin-average of the in
163 situ data in the domain on $0.25^{\circ} \times 0.25^{\circ}$ grid. Figure 2 shows the mean SSS from SMAP
164 L3 and in situ data averaged over the period from April 2015 to Sept. 2016. SMAP SSS
165 agrees reasonably well with in situ, depicting the relatively fresh water in the western
166 Mediterranean in Balearic Sea, with increased salinity moving eastward into Tyrrhenian
167 Sea, and becoming extremely salty along the tracks from Sicily to Suez Canal. The
168 correlation between SMAP and ship data over collocated grid points is 0.78 with bias of
169 0.12 PSU and the standard deviation and Root Mean Square Difference (RMSD) of about
170 0.5 PSU (Table 1).

171 Table 1. Statistical differences between SMAP L3 daily SSS and in situ data in the
172 Mediterranean.

In situ	Bias	Standard deviation	RMSD	Correlation
GOSUD/HMCR	0.12	0.51	0.52	0.78
Argo	-0.29	0.50	0.58	0.70
Argo-Zone 1	0.02	0.47	0.47	0.55
Argo-Zone 2	-0.78	0.41	0.89	0.11
Argo-Zone 3	-0.48	0.39	0.62	0.33

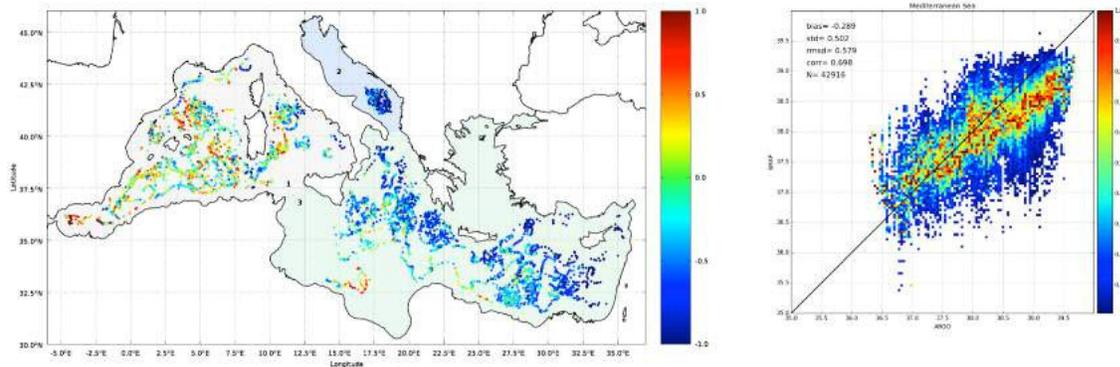
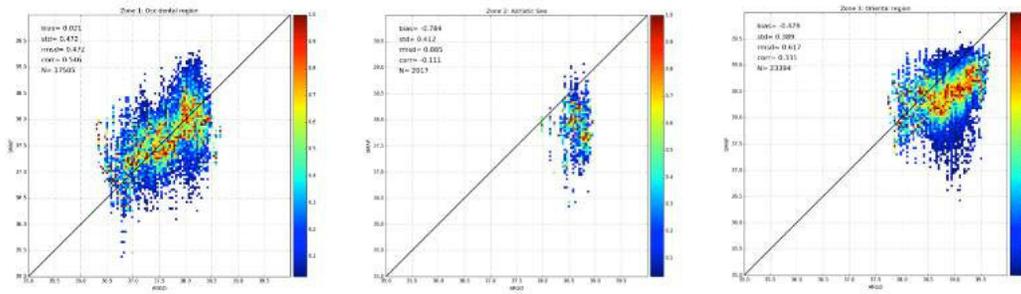


Figure 3. Comparison of SMAP L3 daily and Argo SSS in the Mediterranean during April 4, 2015 and April 3, 2016. (a) Difference map and (b) Density plot. The Mediterranean Sea is divided in the three zones indicated in the figure: Occidental region (zone 1), Adriatic Sea (zone 2) and oriental region (zone 3). Only measurements meeting the constraint: $Q1 - 1.5 \times IQR < |SMAP - Argo| < Q3 + 1.5 \times IQR$ are used to compute statistics. $Q1$ and $Q3$ are the first and third quartile and IQR is the interquartile range ($IQR=Q3-Q1$). Measurements out of this range are considered as outliers, The data from the whole year are used to compute outliers.

173

174 We have compared the daily SMAP L3 SSS with Argo SSS (closest to surface,
 175 cut-off at 10m and collocated with $0.25^\circ \times 0.25^\circ$ grid cell within 8 days) in the
 176 Mediterranean Sea during one year (from April 4, 2015 until April 3, 2016). This is a
 177 region strongly affected by RFI. Nevertheless, only a 2.8% of the SMAP-Argo
 178 comparisons can be considered as outliers [Tukey, 1977] and are mainly concentrated in
 179 the Levantine basin and in the south of the Adriatic Sea (Fig. 3a). By neglecting outlier
 180 measurements, the correlation between SMAP and Argo profiles data is about 0.70 with
 181 bias of -0.29 PSU, the standard deviation about 0.50 and RMS difference of about 0.58
 182 (Fig. 3b). These values are consistent with the statistical differences from GOSUD and
 183 HCMR data (Table 1). It is worth noting that the Argo distribution is conditioned by the
 184 bathymetry, showing a lack of measurements in the Sea of Sicily and the Aegean Sea.



(a) Zone 1

(b) Zone 2

(c) Zone 3

Figure 4. Density plot of SMAP L3 daily maps in front of the corresponding ARGO values for the three regions of the Mediterranean Sea. Data correspond to the period from April 4, 2015 to April 3, 2016.

185 Three regions can be identified depending on the differences between SMAP and
 186 Argo. These regions are shown in Fig. 3a. Inspection of this figure shows that bias of
 187 occidental (zone 1) and oriental (zone 3) regions are different, being larger in the oriental
 188 one. In the oriental region SMAP provides smaller salinity values than Argo. This
 189 difference between three zones is quantified in Fig. 4. The bias in the occidental part is
 190 very small (0.02 PSU) with a standard deviation and an RMSD of 0.47, whereas the
 191 values of the bias, standard deviation and RMSD increase in the oriental region (-0.48,
 192 0.39 and 0.62, respectively). The cause of this difference could be the concentration of
 193 RFI sources in the oriental Mediterranean which is larger than in the occidental region.
 194 The comparison in the Adriatic Sea (zone 2) provide poor results (bias of -0.78, RMSD
 195 of 0.88 and correlation of -0.11), probably due to the fact that it is a coastal sea and land
 196 contamination effects are difficult to correct. A future adjustment of the SMAP RFI
 197 mitigation algorithms and land contamination correction could provide better values in
 198 zones 2 and 3.

199
 200 3.1 Comparison with global monthly gridded Argo data
 201

202 We compare the monthly SMAP L3 SSS with Argo gridded salinity from SIO and
 203 APDRC for the period from April 2015 to September 2016. Fig. 5 shows the global

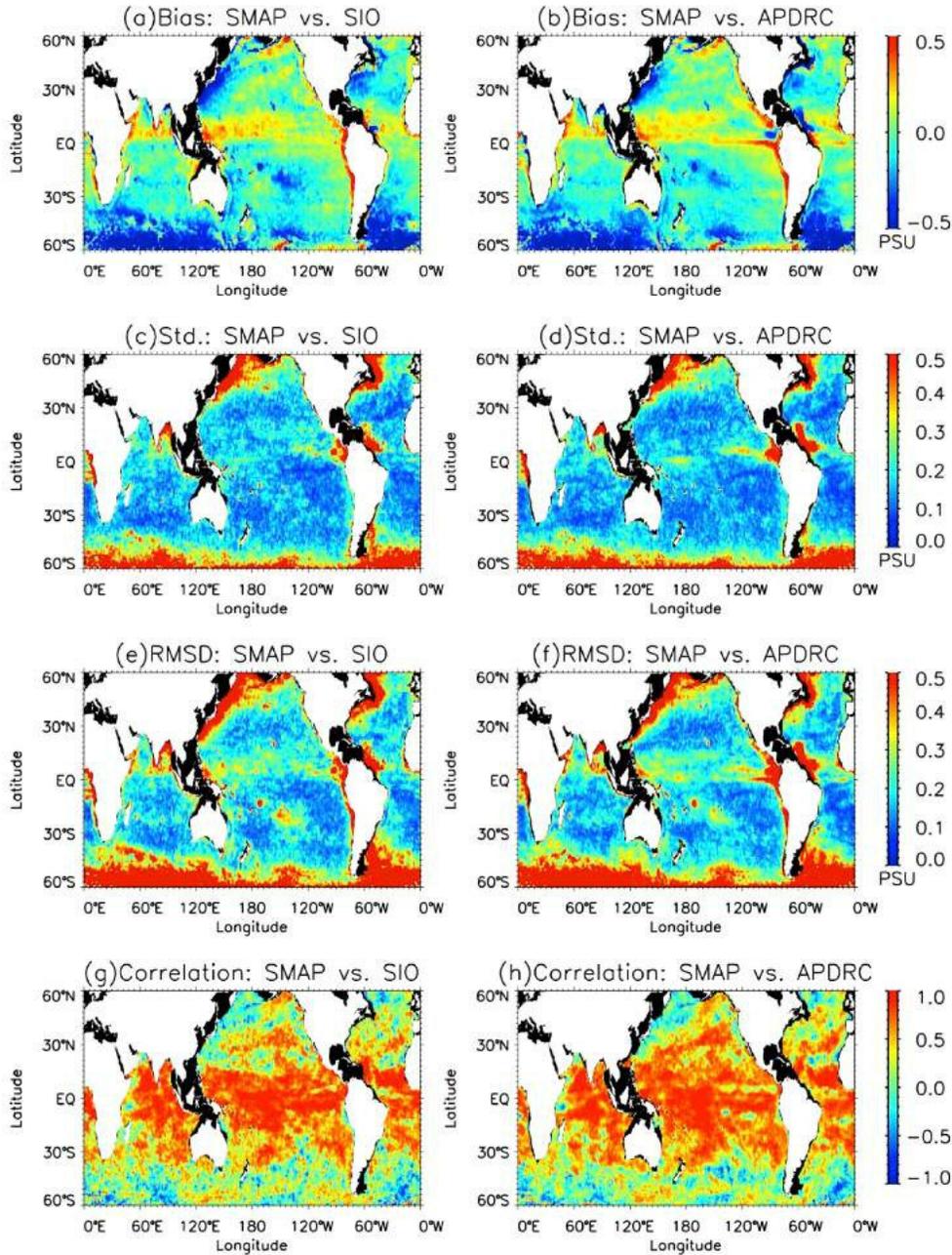


Figure 5. Comparison of SMAP SSS with monthly Argo from SIO (left) and APDRC (right): (a & b) Biases, (c & d) standard deviation, (e & f) RMS difference and (g & h) correlation coefficients.

204 maps of the mean, standard deviation and Root-Mean-Square (RMS) difference of SMAP
205 minus Argo and their correlation coefficients. In the majority part of the tropical oceans
206 away from the coast, SMAP show small error (< 0.2 PSU) and high correlation (> 0.7)
207 with respect to (w.r.t.) Argo data.

208 We can identify several regions where there are noticeable large differences
209 between SMAP and Argo OI products. First in the high latitudes (40° poleward) there is
210 large RMSD or standard deviation (> 0.5 PSU) coincident with low correlation (< 0.5).
211 In addition to large instrument measurement error and significantly reduced L-band
212 radiometer sensitivity to salinity signal in cold water, this may also be caused by the
213 degradation in performance of T_B -only retrieval algorithm under the influence of strong
214 wind and high wave without the use of radar data to assist the roughness correction of
215 excess surface emissivity.

216 Second, large RMS difference are observed in the regions adjacent to land,
217 particularly noticeable along the west coast of Africa and South America, east of North
218 America and Asia, and near Amazon. The substantial negative bias in the coastal oceans
219 of China could be the result of un-mitigated RFI [Mohammed et al., 2016]. Part of those
220 differences could be caused by the error in Argo OI products due to the under-sampling
221 by Argo floats in regions significantly influenced by the spatiotemporal variability
222 associated with boundary currents, river plumes, upwelling, etc.. Along the South
223 America coast near Chili, although RMSD (Fig. 5e & f) is large but the standard
224 deviation (Fig.5c & d) is less than 0.2 PSU. This may suggest error caused by the bias
225 due to the residual error in land contamination correction on SMAP's radiometer data.

226 Third area with large difference is where there could be significant near surface

227 salinity stratification, such as in the Eastern Pacific Fresh Pool (EPFP) where Argo OI
 228 error is small but RMSD/std are large. This is because satellite measures salinity at 1-2
 229 cm near the surface while the majority of Argo floats were turned off within 2-5 m near
 230 the surface. Discrepancy is expected between salinity measured by satellite and Argo
 231 particularly under persistent rainy conditions [Boutin et al., 2015; Tang et al. 2014].

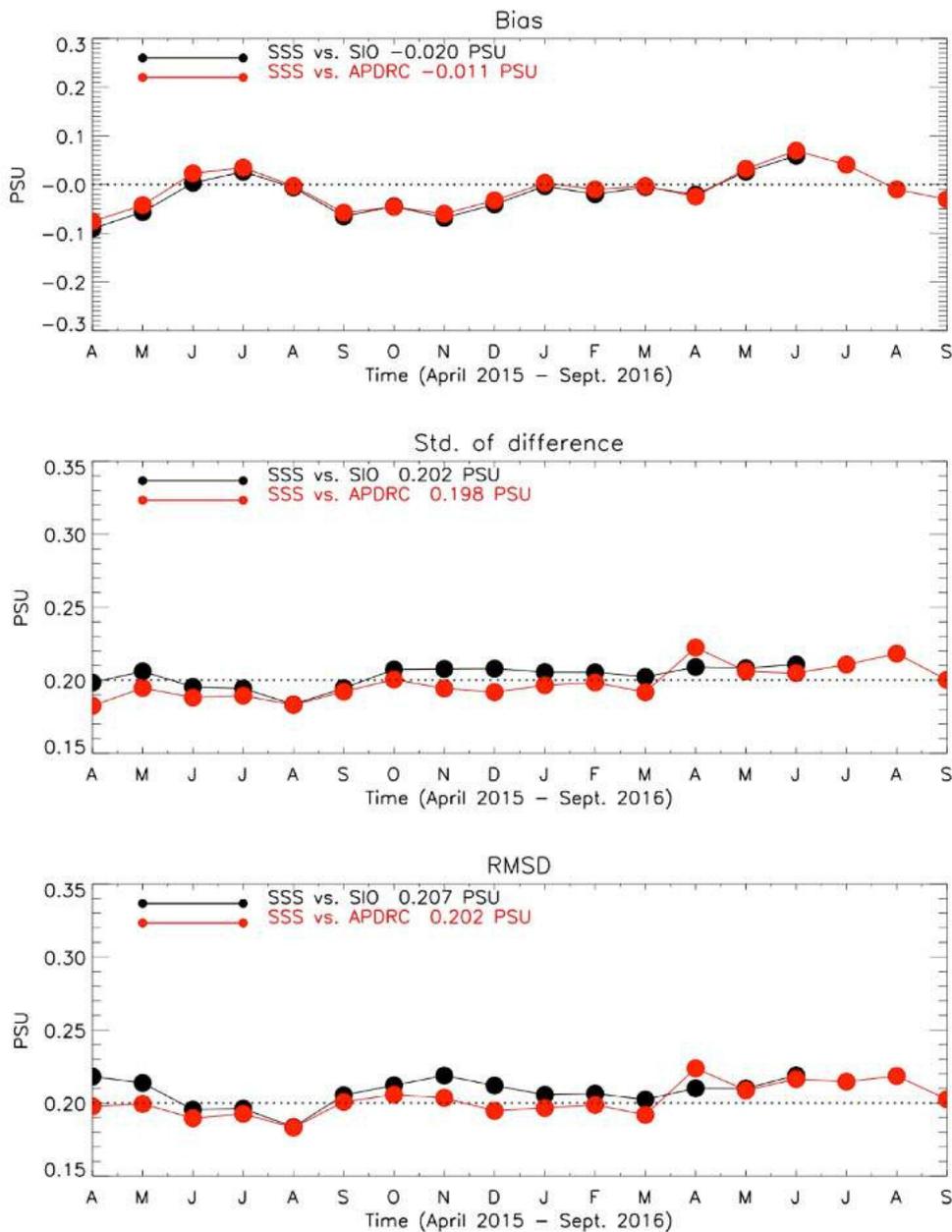


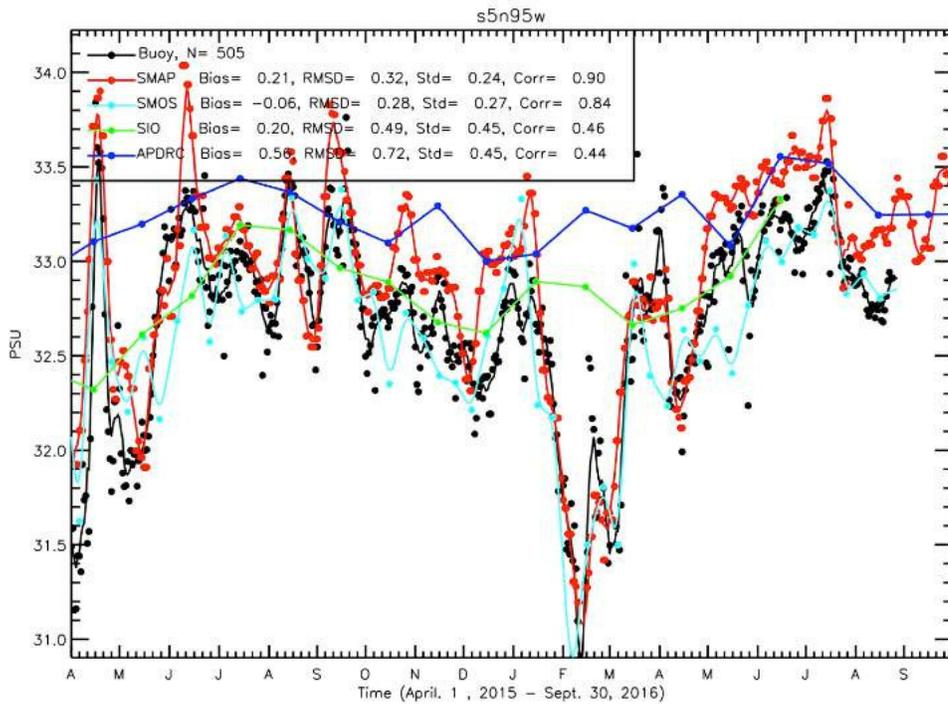
Figure 6. Monthly mean (top), standard deviation (middle) and RMS difference (bottom) between SMAP and Argo from SIO (black) and APDRC (red).

232 In summary, the comparison with Argo monthly gridded data identified regions
233 where (1) satellite retrieval needs improvements (high latitudes), (2) Argo-gridded data is
234 unreliable to be used for assessment (coastal regions), and (3) SMAP SSS differ from
235 salinity measured by Argo due to near-surface stratification. Excluding those areas, we
236 obtain the monthly error assessment between 40°S and 40°N latitudes as shown in Fig. 6.
237 Averaged over the whole period, the bias between SMAP and Argo is near zero with
238 RMS difference around 0.2 PSU.

239 3.2 Comparison with moored buoys in the tropics

240
241 Moored buoy arrays in tropical oceans provide daily salinity measurements at 1 m
242 depth. Daily sampling of buoy data allows us to validate the SMAP data at weekly-
243 biweekly time scale. We extract the time series of data from L3 SMAP and SMOS
244 products at each buoy locations, with a 7-day moving average applied to the time series
245 of each collocation. As an example, Fig. 7 illustrates the time series at the TAO buoy
246 located at 5°N, 95°W and the RAMA buoy at 0°N, 90°E. It demonstrates that SMAP and
247 SMOS SSS products agree well with each other and depict salinity fluctuations very
248 close to the buoy 1 m salinity. Particularly interesting is that SMAP SSS not only closely
249 agrees with buoy data in depicting the more than 2 PSU freshening peaked in Feb. 2016
250 at TAO buoy and Nov. 2015 at RAMA buoy, respectively, but also the timing of rapid
251 fluctuations during the course of salt recovering afterwards. The monthly APDRC and
252 SIO SSS in general corroborate the mean of the SMAP and SMOS SSS. However, they
253 missed or underestimated the fluctuations with time scales shorter than about two months,
254 which are signals that SMAP, SMOS, and mooring data show reasonable agreement.
255 Note that there is a time-varying bias of about 0.1 to 0.5 PSU between APDRC and SIO

(a)



(b)

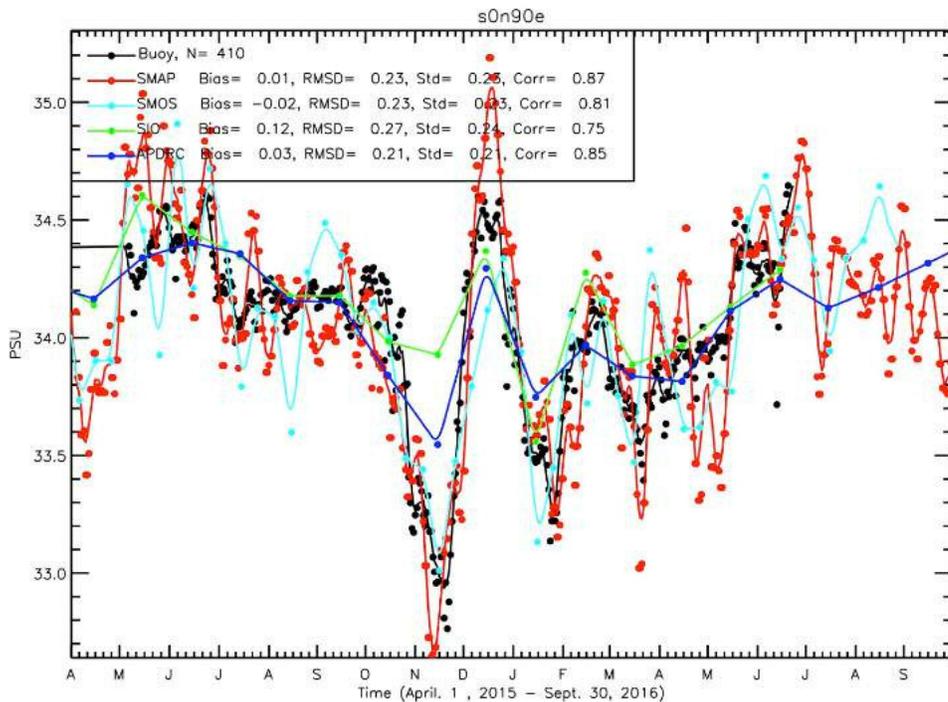


Figure 7. Time series of buoy salinity at 1m depth (black) and collocated SMAP (red) and SMOS (cyan) SSS at (a) TAO buoy location 5°N, 95°W and (b) RAMA buoy location 0°N, 90°E, from April 1, 2015 to Sept. 30, 2016, with 7-day moving average applied, over plotted with monthly Argo data from SIO (green) and APDRC (blue).

257 at 5°N, 95°W, indicating the uncertainty of Argo-gridded products. The agreement
258 between SMAP, SMOS and buoy SSS demonstrates that SMAP salinity has very good
259 skill to track large change of salinity at about weekly time scale.

260 We examined the daily 1 m salinity measured at each moored buoy locations
261 from TAO, PIRATA and RAMA arrays. There are total of 97 buoys each with at least
262 100 daily records collocated with SMAP period. Figure 8 shows the color-coded means,
263 standard deviations, RMS differences and Pearson correlation coefficients between
264 SMAP and buoy. Note the number of collocated pairs between buoy and SMAP varies
265 with locations. SMAP SSS generally agree well with buoys, with temporal correlation at
266 77 out of 97 buoys locations exceeding 0.6, all of which are statistically significant with
267 p-value less than 0.001.

268 There are several buoy sites where large biases and RMSD are observed,
269 including the three locations along 180° in the central Pacific, a few locations in the
270 eastern equatorial Pacific fresh pool and in the BOB along 90°E. At these locations, RFI
271 contamination is not likely to be the main error source as indicated by the RFI probability
272 maps [Mohammed et al., 2016]. We suggest two possible causes for the large discrepancy
273 observed. First it may reflect the expected difference between the point-wise in situ
274 measurements and the satellite observations that represent the averages over its footprints
275 [Vinogradova and Ponte, 2013, Boutin et al. 2015]. For example for the several RAMA
276 buoys along 90°E, the agreement between SMAP and buoys are excellent at three
277 southern locations away from the land (1.5°S, 0°, and 4°N) with RMSD ~0.2 PSU and
278 correlation ~ 0.8, but moving northward into BOB the discrepancy becomes larger with
279 RMSD increased to 0.4 PSU and correlation reduced to 0.6. It is likely that in the BOB

280 where SSS structure is dominated by small spatial variability under the influence of river
 281 runoffs and meso- and submesoscale variability, there can be a larger difference between
 282 the spatial average for satellite measurements with the footprint (~ 40km) and point

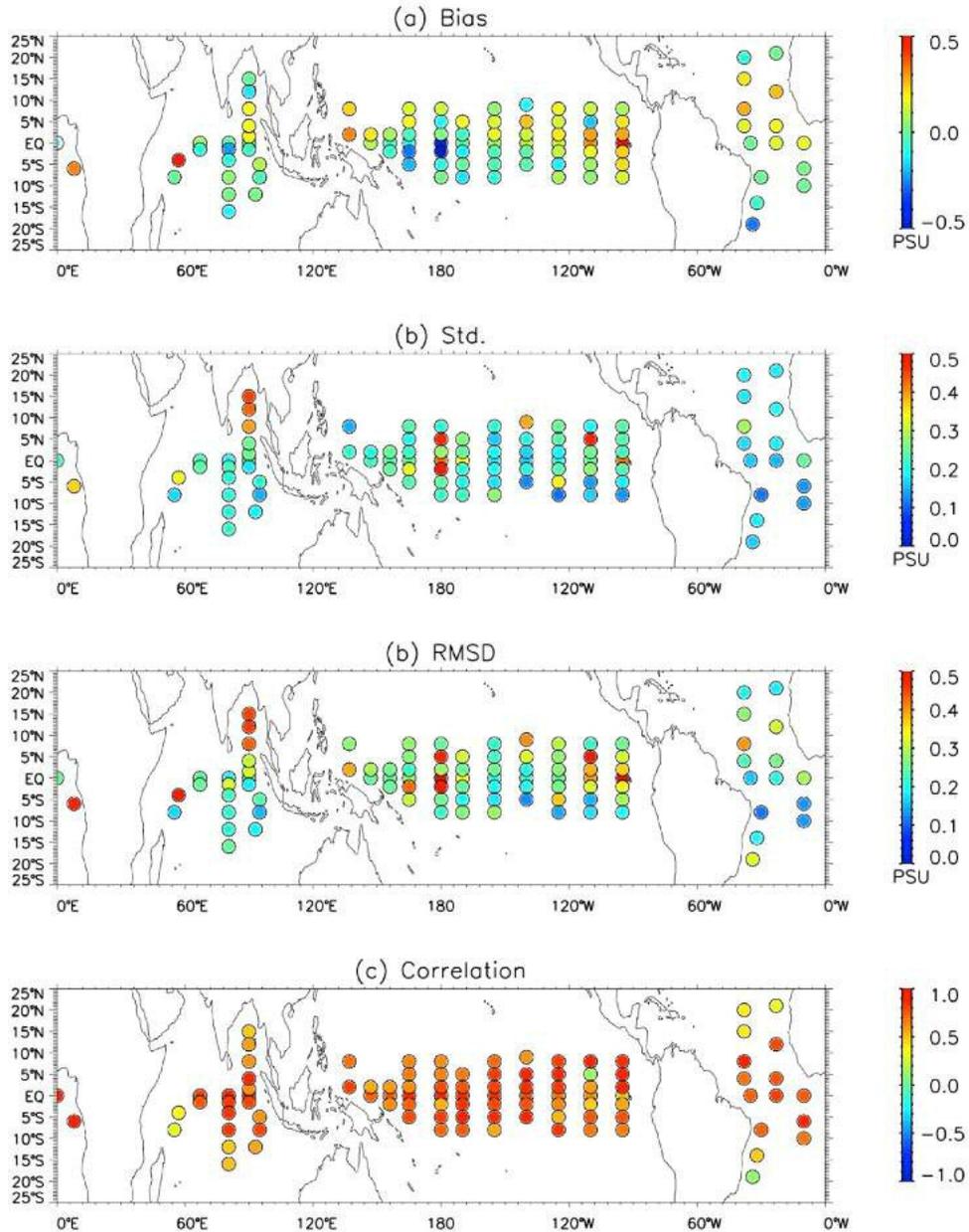
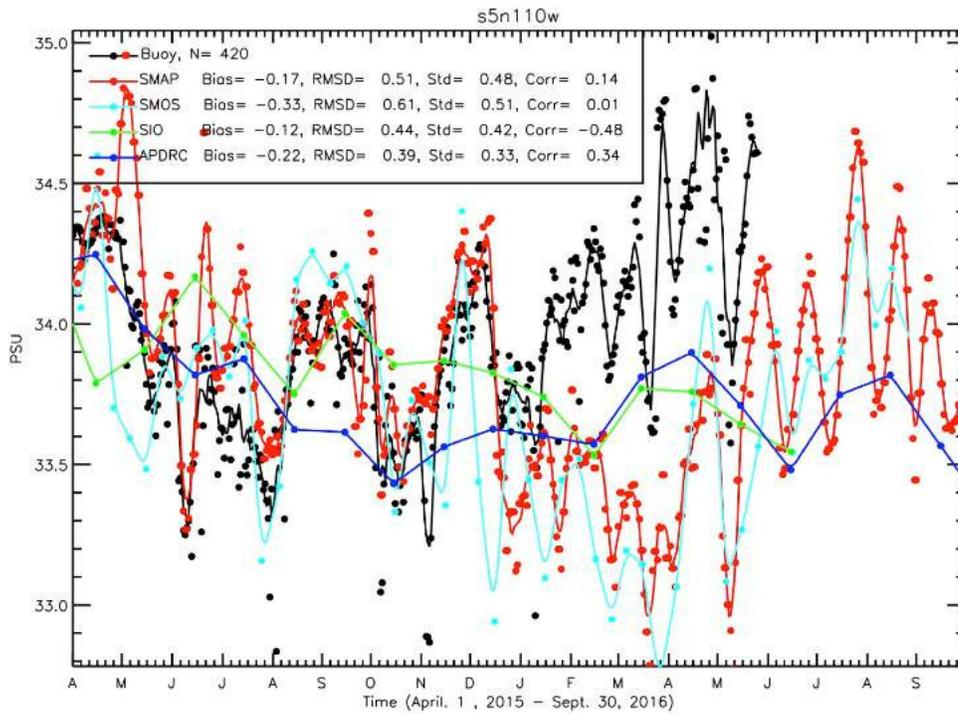


Figure 8. Comparison of SMAP SSS with salinity measured by moored buoys at 1 m depth: (a) Biases, (b) standard deviation, (c) RMS difference and (d) correlation coefficients.

283 measurements by buoy.

284 The second possibility is malfunctioning of buoy salinity sensor and the corrupted
285 real time data were not flagged. One such example is the time series of TAO buoy at 5°N,
286 110°W (Fig.9a), where the real time 1-m salinity from buoy agrees with SMAP and
287 SMOS SSS until Dec. 2015 (the delayed-mode buoy salinity data that have better quality-
288 control flags are not yet available). After Dec. 2015, the mooring salinity became
289 progressively higher. This increase in mooring salinity is inconsistent with the satellite
290 SSS (from SMAP and SMOS) or the Argo products (SIO and APDRC). While buoy
291 salinity drifted away from satellite data by about 1 PSU, it is also interesting to note that
292 the buoy SSS remained to have temporal variation with similar amplitude to SMAP and
293 SMOS. Another example is at TAO location 5°S, 125°W where buoy data suddenly
294 jumped by more than 1 PSU in Sept. 2015 and stay higher than satellite and Argo
295 measurements for the following six months. After March 2016, the buoy salinity values
296 returned to the level agree with all other measurements after the salinity sensor was
297 replaced on March 5, 2016 (Karen Grissom, National Buoy Data Center, personal
298 communication). Clearly, the large standard deviation of the SMAP and buoy differences
299 are essentially caused by the large discrepancy during those periods when buoy data
300 showed suspicious abnormal behavior.

(a)



(b)

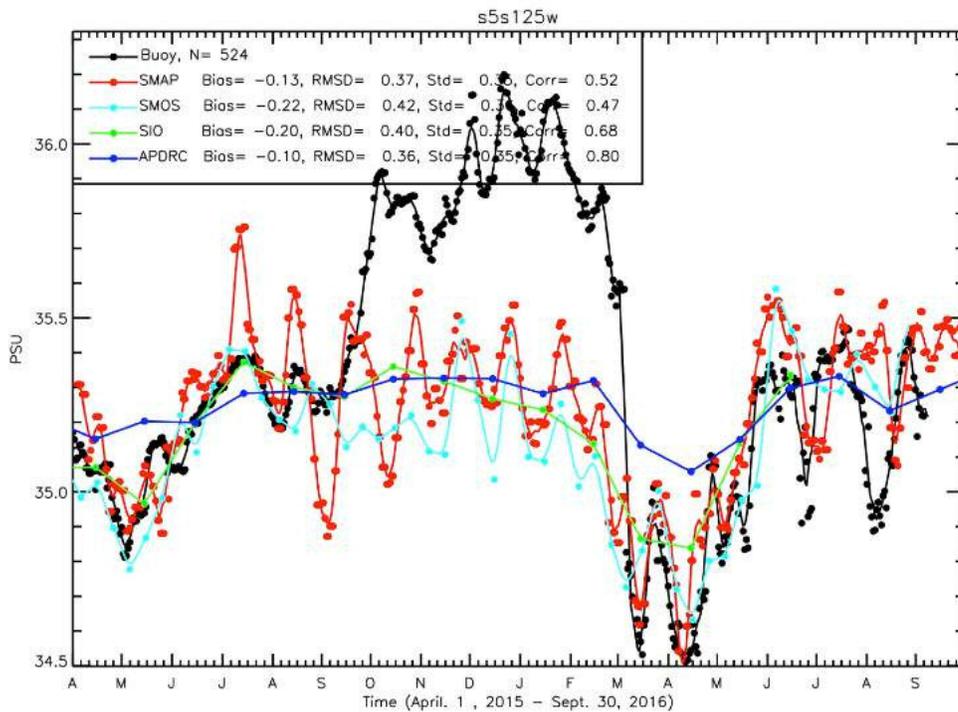


Figure 9. Time series of buoy salinity at 1m depth (black) and collocated SMAP (red) and SMOS (cyan) SSS at TAO buoy location (a) 5°N, 110°W and (b) 5°S, 125°W from April 1, 2015 to Sept. 30, 2016, with 7-day moving average applied, over plotted with monthly Argo data from SIO (green) and APDRC (blue).

302 Table 2. Statistical differences between SMAP L3, SMOS, Argo from SIO, Argo from
 303 APDRC and salinity measured at 1 m by moored buoys.

Dataset	7-day average				30-day average			
	Bias	Standard deviation	RMSD	Correlation	Bias	Standard deviation	RMSD	Correlation
SMAP	0.07	0.22	0.26	0.73	0.05	0.17	0.22	0.80
SMOS	-0.15	0.26	0.26	0.63	-0.16	0.22	0.32	0.71
ARGO _{SIO}	0.04	0.19	0.21	0.72	0.03	0.16	0.19	0.79
ARGO _{APDRC}	0.03	0.20	0.24	0.66	0.03	0.17	0.21	0.71

304
 305
 306 After inspecting the time series of all 97 buoys, we found 10 of them have large
 307 drift or jump in the 1-m salinity time series, in disagreement with SMAP, SMOS and
 308 Argo from SIO or APDRC. These suspicious buoy data, most likely due to malfunctioned
 309 mooring salinity sensors (Meghan Cronin, NOAA/Pacific Marine Environmental
 310 Laboratory, personal communication), were excluded from SMAP SSS assessment. As
 311 listed in Table 2, the bias, standard deviation and RMS difference averaged over the
 312 remain 87 buoys are 0.07, 0.22 and 0.26 PSU on 8-day (~weekly) scale and reduces to
 313 0.05, 0.17 and 0.22 PSU on monthly scale (with 30-days moving average applied). Table
 314 2 also summarizes similar statistical comparisons between moored buoys with SMAP,
 315 SMOS, Argo from SIO and APDRC respectively. Averaged over 87 buoys, SMAP and
 316 Argo products show small biases and similar statistics. The standard deviation and
 317 RMSD between SMAP and buoy is slightly higher than that between Argo and buoy by
 318 less than 0.05 PSU, while the correlation between SMAP and buoy is slightly better than
 319 Argo-gridded on both weekly and monthly scales.

320 The ability of satellite SSS to identify suspicious mooring salinity data as
 321 discussed in relation to Fig. 9 suggests that satellite SSS can be used to perform real-time
 322 quality control (QC) of mooring salinity data. While Argo OI products can also be
 323 potentially used for this purpose, these products missed or underestimated many shorter-

324 term fluctuations (as discussed earlier). This, compounded by the smaller amount of real-
325 time Argo data volume, limits the potential utility of Argo data for real-time QC of
326 mooring salinity.

327

328 3.3 Comparison with STS floats in BOB

329 Figure 10 shows STS salinity on top of SMAP L3 SSS from July 2 to August 12,
330 2016, the period when BoBBLE STS data is available. Collocated data is shown in six
331 consecutive plots, each represents one week of SMAP and STS measurements. The daily
332 STS data are matched up with the closest SMAP L3 grid point and over plotted on the

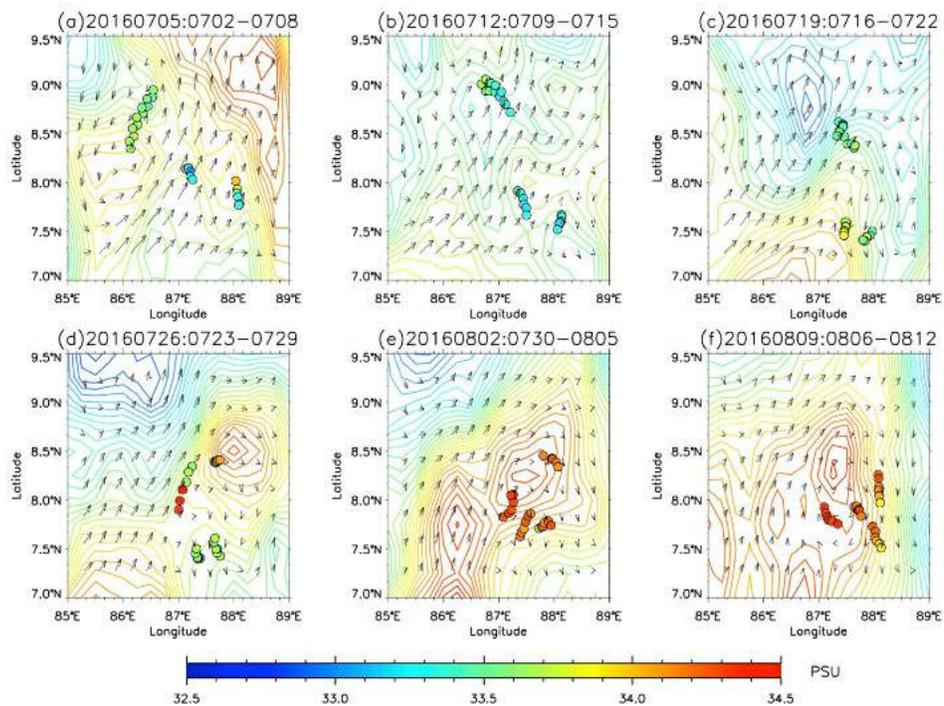


Figure 10. The Argo STS surface salinity data collected during BoBBLE field campaign from July 2 to August 12, 2016 are shown with SMAP L3 SSS for the same period. Each panel contains 7 days of STS data from four Argo floats (color circle) plotted on top of SMAP L3 SSS (color coded contours, offset by 0.4 PSU) and OSCAR currents (black arrows) for the corresponding week.

333 weekly SMAP SSS data, which is produced from SMAP L2 data for the same period.
334 Also shown is the near surface ocean currents from OSCAR (Ocean Surface Current
335 Analysis Real-time, available from <http://podaac.jpl.nasa.gov>). It appears that both
336 SMAP and Argo depicted the salty water intrusion from Arabian Sea to the Bay of
337 Bengal during the Indian Summer Monsoon. The surface salinity in the region jumped
338 about 2 PSU in a few weeks when the salty water entered from the southern BOB in
339 middle of July, transported northward, and spread over the region in early August. SMAP
340 and Argo consistently captured the evolution of rapid salinity change associated with
341 the event. In the third week of July (Fig.10c), SMAP observed the sharp fronts of
342 incoming salty water in southern BOB, when Argo floats happening to be near the fronts
343 showed similar salinity values. The week after (Fig.10d), SMAP showed one patch of
344 salty water moving northward, followed by a new patch of salty water input, while Argo
345 floats situated in between the two patches. From late July to early August, the two
346 patches merged when the floats were in the center of salinity maximum.

347 Figure 11 shows the scatter plots of collocated SMAP SSS and Argo salinity returned
348 respectively by STS and 41-CP, which is averaged from measurements within 5 meters
349 from surface. The comparison between SMAP and STS or 41-CP are quite similar with a
350 standard deviation of about 0.2, RMSD of about 0.5 PSU and correlation exceeding 0.8.
351 It is noted that the agreement with 41-CP is slightly better than STS. It should also be
352 noted that a major part of RMSD is caused by a bias of about 0.45 PSU. We have
353 examined the difference between SMAP and the RAMA buoy located at 8°N and 90°E,
354 which is located slightly to the east of the domain indicated in Fig. 10; we found a small
355 bias of 0.08 PSU at this RAMA buoy location (Fig. 12), much

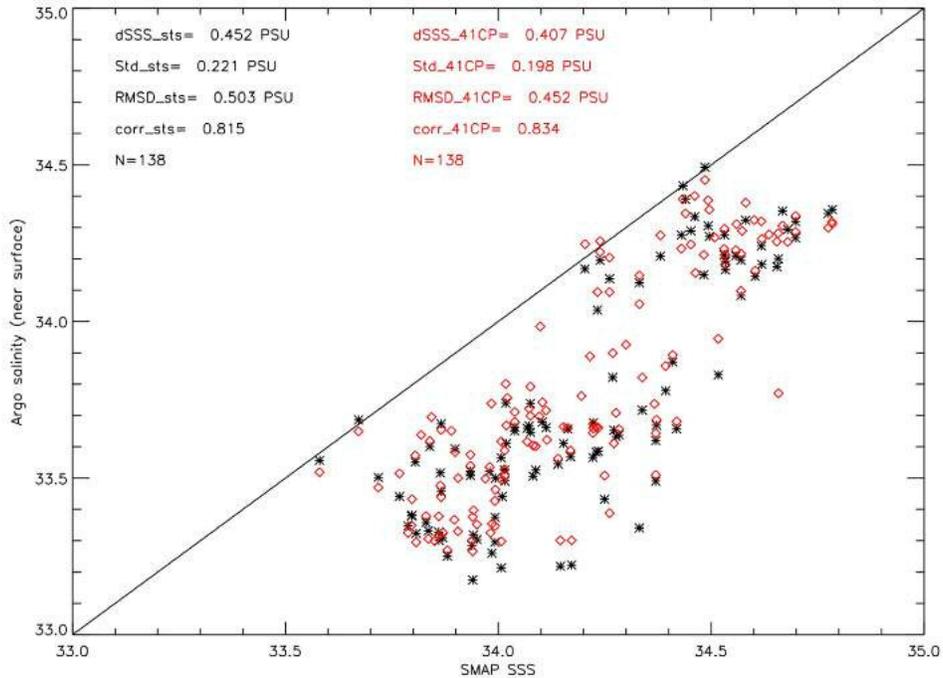


Figure 11. Scatter-plot of SMAP SSS and collocated Argo surface salinity from STS (black) and 41-CP (red).

356 smaller than the 0.5 PSU bias with respect to the STS or 41-CP. This suggests that there
 357 was a near surface salinity stratification with a horizontal gradient from east to west.

358
 359 **4. Conclusions**
 360

361 The SSS retrieved from the SMAP T_B has been validated with in situ measurements
 362 from Argo floats, moored buoys, and TSG data collected by ships on various time scales.
 363 We conclude that SMAP SSS retrieved from L-band radiometer has achieved an accuracy
 364 of 0.2 PSU globally between 40°S and 40°N on a monthly basis through comparison with
 365 Argo gridded data. In tropical oceans, salinity measured at 1 m by moored buoys
 366 indicate SMAP is able to track large salinity changes occurred within month, with RMSD
 367 of 0.26 PSU on weekly scale, which reduced to 0.22 PSU on monthly scale.

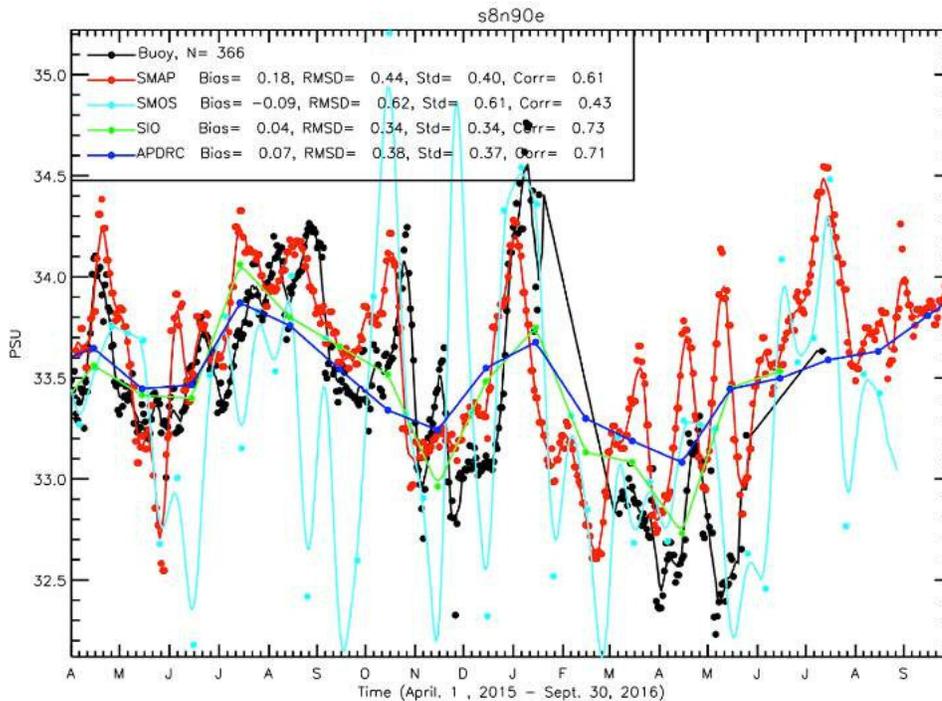


Figure 12. Time series of buoy salinity at 1m depth (black) and collocated SMAP (red) and SMOS (cyan) SSS at TAO buoy location 8°N, 90°E from April 1, 2015 to Sept. 30, 2016, with 7-day moving average applied, over plotted with monthly Argo data from SIO (green) and APDRC (blue).

368 The unique capability of SMAP to observe salinity signals in coastal oceans and
 369 marginal seas is demonstrated through an assessment using TSG data along ship tracks in
 370 the Mediterranean Sea and data collected from floats equipped with STS in BOB. SMAP
 371 reveals features consistent with the in situ measurements: the salinity spatial structure
 372 across the Mediterranean Sea, and sub-monthly evolution of Arabian salty water intrusion
 373 into BOB. The slightly higher RMSD (~0.5 PSU) observed in Mediterranean Sea and
 374 BOB may not only result from the land and RFI contamination on SSS retrieval, but also
 375 due to the limited number of matchups in these regions. A validation with the much more
 376 matchups of SMAP and in situ data, as well as process oriented studies such as
 377 demonstrated in Servain et al. [2016] are needed to provide systematic assessment of
 378 SMAP SSS retrieval in marginal seas and near coast.

379 The validation identified areas with relatively large discrepancy between SMAP and
380 in situ measurements, suggesting future improvements of the T_B -only SMAP retrieval
381 algorithm in the cold water, which tends to be under the influence of strong wind and
382 high wave.

383 Note that the statistics of the differences of SMAP SSS from in-situ salinity
384 measurements not only reflect the uncertainties of SMAP SSS, but also include other
385 factors. These factors include (1) the uncertainties of the Argo IO products (e.g., Lee
386 2016), (2) near-surface salinity stratification (e.g., Boutin et al. 2015), and (3) scale-
387 mismatch between averages on the satellite footprint and point-wise in-situ measurements
388 (e.g., Vinogradova et al. 2013, Boutin et al. 2015).

389 Our time series comparison for SMAP, SMOS, Argo OI products, and mooring data
390 suggest that the satellite SSS have the potential to be used for real-time QC of mooring
391 salinity data to detect measurements that are significantly affected by issues such as
392 biofouling. Satellites, Argo, moorings, and ships provide complementary platforms to
393 monitor global ocean salinity and to assess the associated measurement and sampling
394 errors from different platforms.

395
396 **Acknowledgement**

397 The work described in this paper was carried out by the Jet Propulsion Laboratory,
398 California Institute of Technology under a contract with the National Aeronautics and
399 Space Administration. Argo data were collected and made freely available by the
400 International Argo Program and the national programs that contribute to
401 it (<http://www.argo.ucsd.edu>, <http://www.usgodae.org/argo/argo.html>,
402 <http://argo.jcommops.org>,). The Argo Program is part of the Global Ocean Observing

403 System. Moored buoy data are available from www.pmel.noaa.gov/tao. One of us (JM)
404 acknowledge the support of the Spanish Ministry of Economy and Competitiveness,
405 through the National R+D Plan under PROMISES Project ESP2015-67549-C3-2-R.

406

407

408 **Reference**

409

410 Bourlès, B., R. Lumpkin, M.J. McPhaden, F. Hernandez, P. Nobre, E. Campos, L. Yu, S.

411 Planton, A. Busalacchi, A.D. Moura, J. Servain, and J. Trotte (2008). The PIRATA

412 Program: History, Accomplishments, and Future Directions. *Bull. Amer. Meteor. Soc.*,

413 89, 1111-1125.

414 Boutin, J., Martin, N., Xiaobin, Y., Font, J., Reul, N., & Spurgeon, P. (2012). First

415 assessment of SMOS data over open ocean: Part II; sea surface salinity. *IEEE*

416 *Transactions on Geoscience and Remote Sensing*, 50(5), 1662–1675.

417 Boutin, J., et al. (2015). Satellite and in situ salinity: Understanding near-surface

418 stratification and sub-footprint variability. *Bulletin of the American Meteorological*

419 *Society*. <http://dx.doi.org/10.1175/BAMS-D-15-00032.1>.

420 Boutin, J., N. Martin, N. Kolodziejczyk, and G. Reverdin (2016). Interannual anomalies

421 of SMOS sea surface salinity. *Remote Sensing of Environment* 180, 128-136.

422 Entekhabi, D., E. G. Njoku, P. E. O’Neill, K. H. Kellogg, W. T. Crow, W. N. Edelstein,

423 J. K. Entin, S. D. Goodman, T. J. Jackson, J. Johnson, J. Kimball, J. R. Piepmeier, R.

424 D. Koster, N. Martin, K. C. McDonald, M. Moghaddam, S. Moran, R. Reichle, J. C.

425 Shi, M. W. Spencer, S. W. Thurman, L. Tsang, and J. Van Zyl (2010). The Soil

426 Moisture Active Passive (SMAP) Mission, *Proceedings of IEEE*, Vol. 98, No. 5, pp.

427 704-716.

428 Font, J., Camps, A., Borges, A., Martin-Neira, M., Boutin, J., Reul, N., ... Mecklenburg,
429 S. (2010). SMOS: The challenging sea surface salinity measurement from space.
430 Proceedings of the IEEE, 98(5), 649–665.

431 Fore, A., S. Yueh, W. Tang, B. Stiles, and A. Hayashi (2016). Combined Active/Passive
432 Retrievals of Ocean Vector Wind and Sea Surface Salinity with SMAP, *IEEE Trans.*
433 *Geoscience and Remote Sensing*, (??) doi: 10.1109/TGRS.2016.2601486.

434 Fournier, S., J. T. Reager, T. Lee, J. Vazquez-Cuervo, C. H. David, and M. M. Gierach,
435 (2016). [SMAP observes flooding from land to sea: The Texas event of 2015](#),
436 [Geophys. Res. Lett.](#), 43, doi:10.1002/2016GL070821.

437 Freitag, H. P., M. E. McCarty, C. Nosse, R. Lukas, M. J. McPhaden, and M. F. Cronin
438 (1999). COARE Seacat data: Calibrations and quality control procedures, NOAA
439 Tech. Memo. ERL PMEL-115, 89 pp. [Available at
440 <http://www.pmel.noaa.gov/pubs/PDF/frei2034/frei2034.pdf>.]

441 Kerr, Y. H., et al. (2010). The SMOS mission: New tool for monitoring key elements of
442 the global water cycle. Proceedings of the IEEE, 98(5), 666–687.

443 Lagerloef, G., F. R. Colomb, D. Le Vine, F. Wentz, S. Yueh, C. Ruf, J. Lilly, J. Gunn, Y.
444 Chao, A. deCharon, G. Feldman, and C. Swift (2008). The Aquarius/Sac-D Mission:
445 Designed To Meet The Salinity Remote-Sensing Challenge, *Oceanography*, Vol. 21,
446 no. 1, Special Issue: Sp. Iss. SI, pp. 68-81.

447 Larson, N. L., C. D. Janzen, and D. J. Murphy (2008). STS: An in- strument for
448 extending ARGO temperature and salinity measurements through the sea surface.
449 2008 Ocean Sciences Meeting, Orlando, FL, American Society of Limnology and
450 Oceanography. [Available online at <http://www.seabird.com/>

451 technical_references/SSalOceanSciencesMar08-5Pages.pdf.]

452 Le Vine, D. M., G. S.E. Lagerloef, F.R. Colomb, S.H. Yeh, and F.A. Pellerano (2007).
453 Aquarius: An instrument to monitor sea surface salinity from space. *IEEE Trans.*
454 *Geosci. Remote Sens.*, 45, 2040–2050.

455 Lee, T. (2016). Consistency of Aquarius sea surface salinity with Argo products on
456 various spatial and temporal scales, *Geophys. Res. Lett.*, 43, 3857–3864,
457 doi:10.1002/2016GL068822.

458 Matthews, A. et al. (2015). BoBBLE: Bay of Bengal Boundary Layer Experiment.
459 CLIVAR Exchanges No. 68, Vol. 19, No. 3, pp 38-42, Nov. 2015.

460 McPhaden, M. J. (1995). The TAO array is completed. *Bull. Amer. Meteor. Soc.*, 76,
461 739–741.

462 McPhaden, M.J., A.J. Busalacchi, R. Cheney, J.R. Donguy, K.S. Gage, D. Halpern, M. Ji,
463 P. Julian, G. Meyers, G.T. Mitchum, P.P. Niiler, J. Picaut, R.W. Reynolds, N. Smith,
464 K. Takeuchi (1998). The Tropical Ocean-Global Atmosphere (TOGA) observing
465 system: A decade of progress. *J. Geophys. Res.*, 103, 14,169-14,240.

466 McPhaden, M.J., and Coauthors (2009). RAMA: The Research Moored Array for
467 African–Asian–Australian Monsoon Analysis and Prediction. *Bull. Amer. Meteor.*
468 *Soc.*, 90, 459–480.

469 Mohammed, P. N., M. Aksoy, J. R. Piepmeier, J. T. Johnson, and A. Bringer (2016).
470 SMAP L-band Radiometer: RFI Mitigation Prelaunch Analysis and First Year On-
471 Orbit Observations, *IEEE Geosci. Remote Sens.*, Vo. 54, No. 10, pp. 6035-6047, Oct
472 2016, doi: 10.1109/TGRS.2016.2578048.

473 Roemmich, D., and the Argo Steering Team (2009). Argo: The challenge of continuing10

474 years of progress, *Oceanography*, 22, 46–55.

475 Servain, J., A. Busalacchi, M. McPhaden, A. Moura, G. Reverdin, M. Vienna, and S.
476 Zebiak (1998). A Pilot Research Moored Array in the Tropical Atlantic (PIRATA).
477 *Bull. Amer. Meteor. Soc.*, 79, 2019–2031.

478 Tang, W., S. Yueh, A. Fore, G. Neumann, A. Hayashi, and G. Lagerloef (2013). The rain
479 effect on Aquarius’ L-band sea surface brightness temperature and radar backscatter.
480 *Remote Sensing of Environment*, 137, 147-157.

481 Tang, W., S. H. Yueh, A. G. Fore, and A. Hayashi (2014). Validation of Aquarius sea
482 surface salinity with in situ measurements from Argo floats and moored buoys, *J.*
483 *Geophys. Res. Oceans*, 119, 6171–6189, doi:10.1002/2014JC010101.

484 Tang, W., S. H. Yueh, A. Hayashi, A. G. Fore, W. L. Jones, A. Santos-Garcia, and M. M.
485 Jacob (2015). Rain-induced near surface salinity stratification and rain roughness
486 correction for Aquarius SSS retrieval. *The Special Issue of the IEEE Journal of*
487 *Selected Topics in Applied Earth Observations and Remote Sensing (J-STARS)*
488 “Aquarius/SACD mission calibration/validation performance and retrieval
489 algorithms”, 8 (12), 5474-5484, DOI: 10.1109/JSTARS.2015.2463768.

490 Tukey, J.W. (1977). *Exploratory data analysis*. Addison-Wesley.

491 Vinogradova, N. T., and R. M. Ponte (2013). Small-scale variability in sea surface
492 salinity and implications for satellite-derived measurements, *J. Atmos. Oceanic*
493 *Technol.*, 30, 2689–2694, doi:10.1175/JTECH-D-13-00110.1.

494 Yueh, S. H., W. Tang, A. Fore, G. Neumann, A. Hayashi, A. Freedman, J. Chaubell, and
495 G. Lagerloef (2013). L-band Passive and Active Microwave Geophysical Model
496 Functions of Ocean Surface Winds and Applications to Aquarius Retrieval. *IEEE*

497 *Trans. Geoscience and Remote Sensing*, 51(9), 4619-4632, DOI:
498 10.1109/TGRS.2013.2266915.

499 Yueh, S. H., W. Tang, A. Fore, A. Hayashi, Y. T. Song, and G. Lagerloef (2014).
500 Aquarius geophysical model function and combined active passive algorithm for
501 ocean surface salinity and wind retrieval, *J. Geophys. Res. Oceans*, 119, 5360–5379,
502 doi:10.1002/2014JC009939.

503 Yueh, S. H., A. Fore, W. Tang, A. Hayashi, B. Stiles, N. Reul, Y. Weng and F. Zhang
504 (2016). SMAP L-Band Passive Microwave Observations Of Ocean Surface Wind
505 During Severe Storms, *IEEE Trans. Geoscience and Remote Sensing*, doi:
506 10.1109/TGRS.2016.2600239.